iScience

CellPress
OPEN ACCESS

Article

Predictive energetic tuning of C-Nucleophiles for the electrochemical capture of carbon dioxide

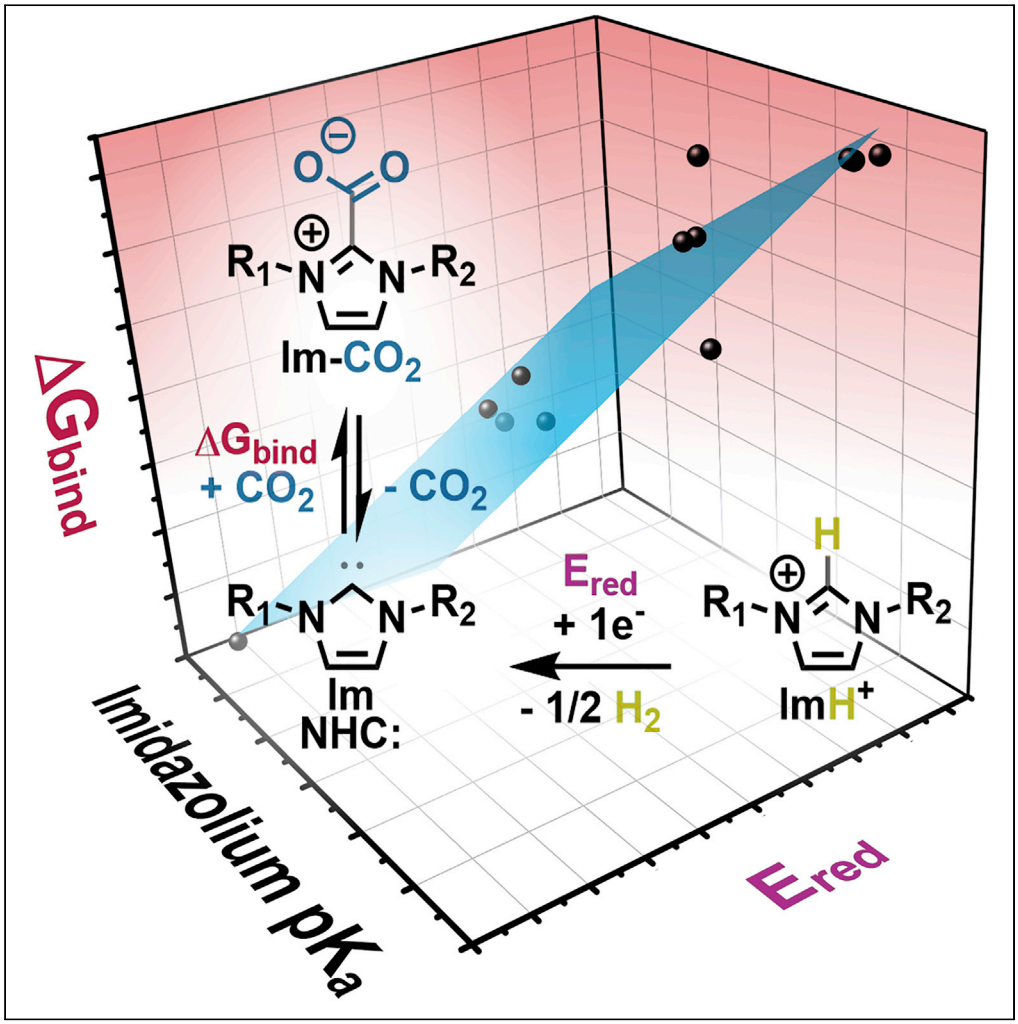

Haley A. Petersen, Abdulaziz W. Alherz, Taylor A. Stinson, Chloe G. Huntzinger, Charles B. Musgrave, Oana R. Luca

charles.musgrave@colorado.edu (C.B.M.)
oana.luca@colorado.edu (O.R.L.)

Highlights

CO_2 binding energy was calculated for a set of N-heterocyclic carbenes (NHCs)

CO_2 binding energy of NHCs is widely synthetically tunable

pK_a, reduction potential, and CO_2 binding energy correlate linearly for NHCs

3D correlation enables easy prediction of CO_2 binding strength for novel NHCs

Petersen et al., iScience 25, 103997
April 15, 2022
https://doi.org/10.1016/j.isci.2022.103997

iScience

CellPress
OPEN ACCESS

Article

Predictive energetic tuning of C-Nucleophiles for the electrochemical capture of carbon dioxide

Haley A. Petersen,[1,4] Abdulaziz W. Alherz,[2,4] Taylor A. Stinson,[1] Chloe G. Huntzinger,[1] Charles B. Musgrave,[1,2,3,*] and Oana R. Luca[1,5,*]

SUMMARY

This work maps the thermodynamics of electrochemically generated C-nucleophiles for reactive capture of CO_2. We identify a linear relationship between the pK_a, the reduction potential of a protonated nucleophile (E_{red}), and the nucleophile's free energy of CO_2 binding (ΔG_{bind}). Through synergistic experiments and computations, this study establishes a three-parameter correlation described by the equation $\Delta G_{bind} = -0.78pK_a + 4.28E_{red} + 20.95$ for a series of twelve imidazol(in)ium/N-heterocyclic carbene pairs with an R^2 of 0.92. The correlation allows us to predict the ΔG_{bind} of C-nucleophiles to CO_2 using reduction potentials or pK_as of imidazol(in)ium cations. The carbenes in this study were found to exhibit a wide range CO_2 binding strengths, from strongly CO_2 binding to nonspontaneous. This observation suggests that the ΔG_{bind} of imidazol(in)ium-based carbenes is tunable to a desired strength by appropriate structural changes. This work sets the stage for systematic energetic tuning of electrochemically enabled reactive separations.

INTRODUCTION

Lowering atmospheric concentrations of CO_2 to levels that will mitigate the effects of climate change will require substantial implementation of carbon-neutral and carbon-negative technologies, including carbon capture (Institute, 2020; National Academies of Sciences, Engineering, and Medicine, 2019). The development of optimal carbon capture materials requires a careful balance of the energetics of CO_2 binding to the proposed capture material. However, CO_2 binding free energies (ΔG_{bind}) are not easily experimentally accessible.

Among proposed materials for CO_2 capture and conversion, imidazolium salts have gained considerable attention due to the attractive liquid properties of their alkylated variants, including their favorable solvation of CO_2 gas as well as their high conductivity, which renders them uniquely suited for electrochemical applications (Kelemen et al., 2011; Sowmiah et al., 2009; Zhao et al., 2016). In addition to these favorable properties, imidazolium salts readily yield N-heterocyclic carbenes (NHCs) through deprotonation (Scheme 1B). Interestingly, electrochemical access to the free NHCs has been previously demonstrated as shown in Scheme 1A. Upon reduction, an imidazolium cation releases half of aH_2 equivalent and becomes a free NHC (Gorodetsky et al., 2004). The free NHC then exhibits reactivity with CO_2, as shown in Scheme 1C. Historically, the reaction of Scheme 1C was originally developed as a protection method for reactive NHCs (Voutchkova et al., 2007), and it has found applications in the synthesis of organometallics (Hahn and Jahnke, 2008) and catalysis (Luca and Fenwick, 2015; Luca et al., 2015; Riduan et al., 2009; Yang and Wang, 2014).

Using this reactivity, we now demonstrate a three-way correlation between the experimentally accessible reduction potential (E_{red}) of the imidazolium (Scheme 1A), the pK_a of the imidazolium (Scheme 1B), and the CO_2 binding energy of the corresponding NHC (Scheme 1C). While the correlation between the pK_a of an imidazolium (Scheme 1B) and ΔG_{bind} of the corresponding free NHCs (Scheme 1C) has been studied using density functional theory (DFT) on a set of 90 imidazoliums (Wang et al., 2018), it has not been related to the E_{red} of the imidazolium (Scheme 1A), which is a property that is routinely measured by standard electrochemical experiments (Gorodetsky et al., 2004). While the number of the imidazolium salts in this study is smaller (Figure 1), we map a landscape of CO_2 binding free energies spanning 15 kcal, 20 pK_a units, and 1.7 V of potential.

[1]Department of Chemistry and Renewable and Sustainable Energy Institute, University of Colorado Boulder, Boulder, CO 80309, USA

[2]Department of Chemical and Biological Engineering, University of Colorado, Boulder, CO 80309, United States

[3]Materials Science and Engineering Program, University of Colorado, Boulder, CO 80309, United States

[4]These authors contributed equally

[5]Lead contact

*Correspondence: charles.musgrave@colorado.edu (C.B.M.), oana.luca@colorado.edu (O.R.L.)

https://doi.org/10.1016/j.isci.2022.103997

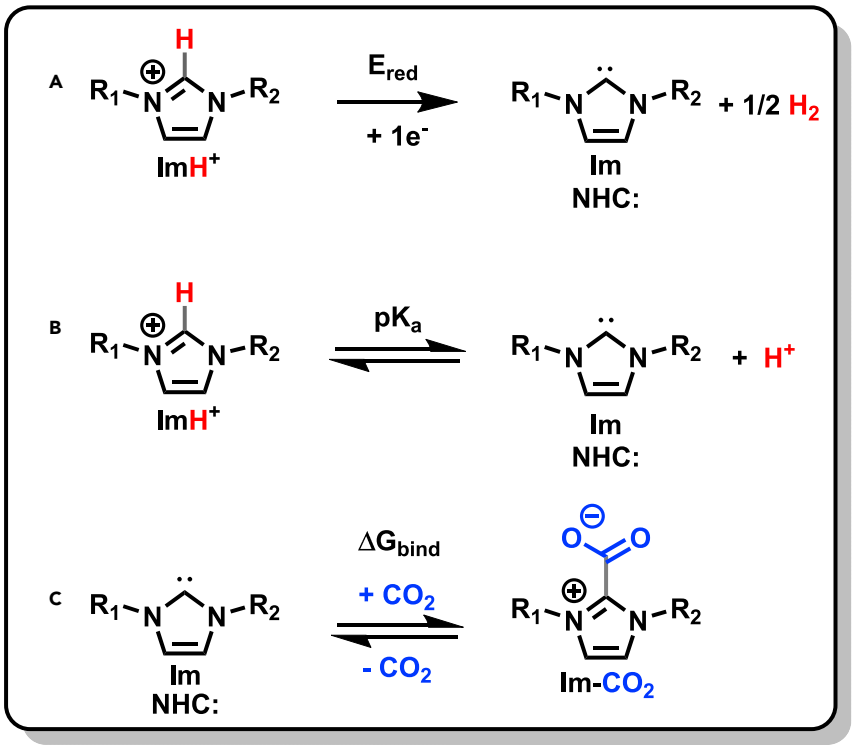

Scheme 1. Reactions of imidazolium cations

Generation of NHCs (Im) from their imidazolium precursors (A and B) and Im binding to CO_2 (C) along with the three properties associated with these reactions: (A) E_{red}, (B) pK_a, and (C) ΔG_{bind}. R_1 and R_2 substituents are described in Figure 1.

We investigate the relationship between E_{red}, pK_a, and ΔG_{bind} associated with reactions A–C in Scheme 1. The parameters are related due to their mutual dependence upon the electron density at the apical imidazolium carbon. Basicity and nucleophilicity are intrinsically related, with basicity being a subset of nucleophilicity. All nucleophiles are Lewis bases, but the term nucleophilicity is utilized to describe the affinity of a molecule to not only protons but also other electron-deficient molecules such as carbon dioxide. In essence, our correlation of pK_a with the free energy of CO_2 binding ranks the nucleophilicity of an NHC against two types of electrophiles: protons and carbon dioxide.

Increasing the electron density of an imidazolium core causes it to have a more negative E_{red} (Scheme 1A); a rise in electron density at a site of deprotonation lowers the stability of the deprotonated species and thus increases the pK_a of the conjugate acid(Scheme 1B); and finally, a rise in electron density on a nucleophile corresponds to an increase in its nucleophilicity and thus its ability to attack an electrophile such as CO_2 is enhanced (Scheme 1C). Although we describe these general relationships to assert that the E_{red}, pK_a, and ΔG_{bind} of the twelve imidazol(in)ium cations presented in Figure 1 are correlated, analogous relationships generally apply to other potential molecular CO_2 capture substrates and thus the approach we use herein may be applied to other, more complex systems for redox-enabled CO_2 capture, such as quinones and N-nucleophiles (Wilcox, 2020). Unlike traditional electroswing systems which operate through cycles of binding CO_2 with cathodically generated nucleophiles followed by release of CO_2 in an electrochemical oxidation step, the electrochemical step of NHC generation and binding of CO_2 can be coupled with a thermal release step rather than an oxidation. The thermal release of CO_2 from NHC adducts is known (Van Ausdall et al., 2009; Luca and Fenwick, 2015), thus setting the stage for hybrid electrothermal CO_2 capture-release methodologies.

RESULTS

Before performing DFT calculations to investigate the relationship between free energy of CO_2 binding, reduction potential, and pK_a for the set of imidazolium cations, we first sought to experimentally validate

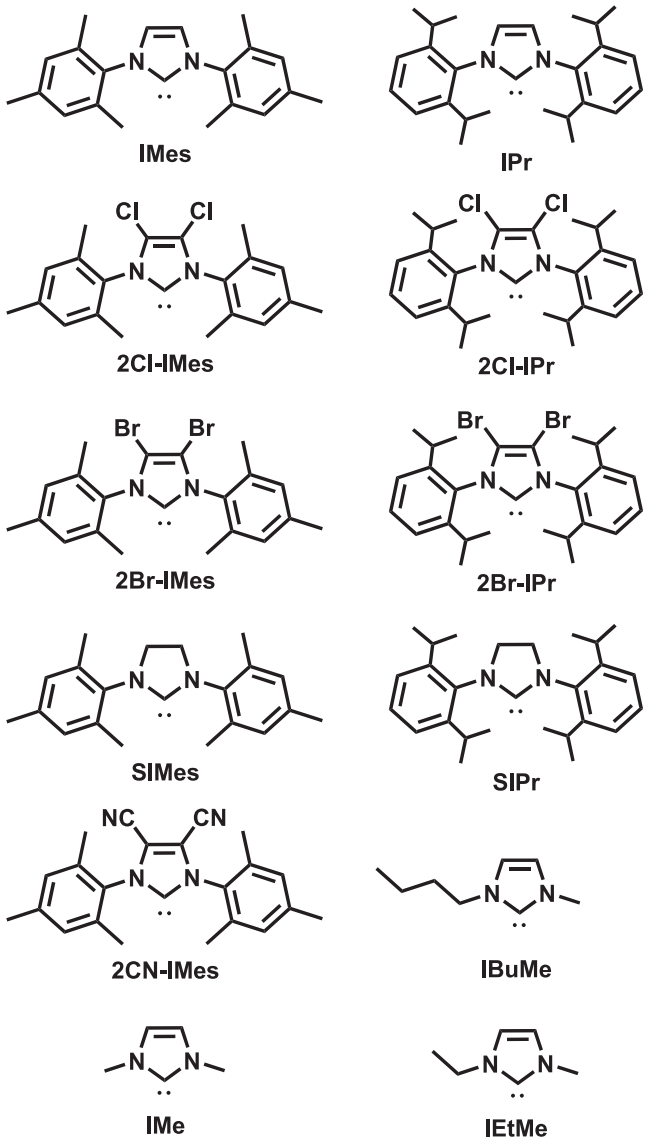

Figure 1. Imidazol(in)ium-based NHCs used in the correlation studies

Structures of each compound under study. See also Figure S1 and Table S1 for applicable experimental values associated with each NHC. Imidazolium counterparts (protonated NHCs) are abbreviated as "NHC"H in this work.

several assumptions about the system. Because imidazolium cations ImH^+ are aromatic, the reduction of ImH^+ to add an electron to the imidazolium π-system results in de-aromatization of the imidazolium ring. Prior studies have shown that aromatic hydrides exhibit a linear correlation between the first reduction potential of the oxidized hydride and the nucleophilicity of the hydride (Alherz et al., 2018; Ilic et al., 2018). To verify this correlation for imidazolium salts, we measured E_{red} for a family of imidazolium salts (Figure S1 and Table S1) using normal pulse voltammetry (NPV). While the influence of ion pairing and association on properties of imidazolium salts has been well documented in the ionic liquid literature (Tsuzuki et al., 2013; Voroshylova et al., 2018; Wang et al., 2015), the nature of the counterion's effects on our measurements is minimized through the use of NBu_4PF_6, an electrolyte with a chemically stable, non-coordinating PF_6^- anion. Furthermore, we validated the observation that one-electron reductions of imidazolium cations produce free NHCs and verified that this applies to the analogous imidazolinium cations with non-aromatic, saturated backbones. We confirmed that the voltammetry responses of imidazolinium cations are associated with one e^- reductions using the method of Donadt et al. (Donadt et al., 2018) based on diffusion ordered spectroscopy (DOSY NMR) and NPV to quantify the number of electrons associated with the

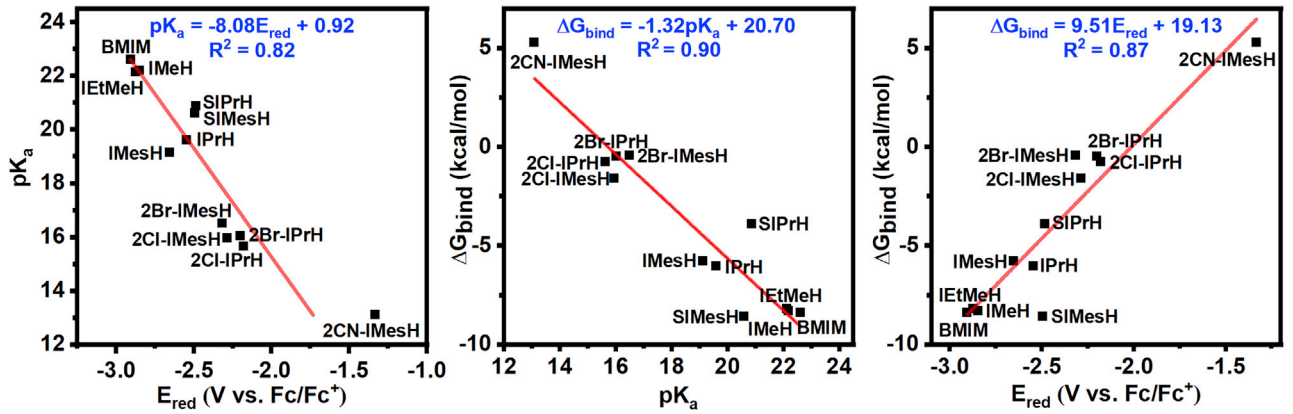

Figure 2. Linear correlations of pK_a, free energy of CO_2 binding, and reduction potential

The three linear two-way correlations of (left) reduction potential and pK_a, (middle) free energy of CO_2 binding and pK_a, and (right) reduction potential and free energy of CO_2 binding for the compounds under study. Optimized molecular coordinates are available in Data S1.

assumed one-electron reduction step (Scheme 1A and Figure S2); this is consistent with the observed one e^- reduction of imidazolium cations to produce free NHCs.

With these experimental validations in hand, we next computed the values of E_{red}, pK_a, and ΔG_{bind} for each of the imidazolium derivatives using DFT based on the MN15/6-311+G(d,p) level of theory paired with the SMD solvent model as implemented in the Gaussian 16 quantum chemistry code (Frisch et al., 2016; Krishnan et al., 1980; Marenich et al., 2009; McLean and Chandler, 1980; Yu et al., 2016). The DFT-computed pK_a and E_{red} values we obtained agree with experiment (Chu et al., 2007; Dunn et al., 2017), with mean absolute errors (MAE) below 0.15 pK_a units and 0.05 V, respectively. For additional computational details, please refer to the STAR methods, Figure S3 and S4, Tables S2–S4.

The calculated free energies of binding to CO_2 range from +5 to −10 kcal/mol, indicating that the equilibrium constant for CO_2 binding varies by over 10 orders of magnitude at 298 K. Consequently, this energy window suggests that the thermodynamics of NHC binding to CO_2 can be tuned over a wide range, for instance, by functionalization of NHCs with appropriate substituents to yield carbenes that bind CO_2 weakly or even nonspontaneously (e.g. 2CN-IMes) to strongly (e.g. Butyl-methyl imidazolium BMIM). Notably, our calculations predict that four carbenes known to be stable in the presence of oxygen (2Cl-IMes, 2Br-IMes, 2Cl-IPr, and 2Br-IPr) (Arduengo et al., 1997; Furfari et al., 2015) have slightly negative values of ΔG_{bind} (−1.60 kcal/mol, −0.43 kcal/mol, −0.76 kcal/mol, and −0.50 kcal/mol, respectively). This observation has implications for direct air capture (DAC) of carbon dioxide, where stability to oxygen is a critical prerequisite for candidate materials. Weak CO_2 binders have an advantage for DAC processes whose thermodynamic efficiency also depends on low-energy release of CO_2 from the sorbent material (Lackner, 2013; Petersen and Luca, 2021).

Computations were then used to investigate three sets of correlations based on reactions a–c of Scheme 1 for twelve imidazol(in)ium cations. Figure 2 includes imidazolium cations that are not easily synthetically accessible. In these cases, correlations were performed using the calculated DFT values for E_{red} and pK_a.

For imidazol(in)ium cations with known pK_a or E_{red}, estimated ΔG_{bind} for the corresponding NHC are readily obtained using the equations produced by the linear regressions shown in Figure 2. For instance, the ΔG_{bind} in kcal/mol of the commercially available NHC precursor IMesH is estimated from either Equations 1 or 2:

$$\Delta G_{bind} = 9.51 E_{red} + 19.13 \quad \text{Equation 1}$$

$$\Delta G_{bind} = -1.32 pK_a + 20.70 \quad \text{Equation 2}$$

In the case of Equation 1, an experimental E_{red} for the compound is obtained within minutes using a routine electrochemical experiment such as NPV. Using the E_{red} value we measured of −2.64 V vs. Fc/Fc^+ for IMesH, we then obtained an estimated ΔG_{bind} for CO_2 binding from Equation 1 of −5.94 kcal/mol. Similarly, with a known pK_a value of IMesH in DMSO of 19.4(Wang et al., 2018), Equation 2

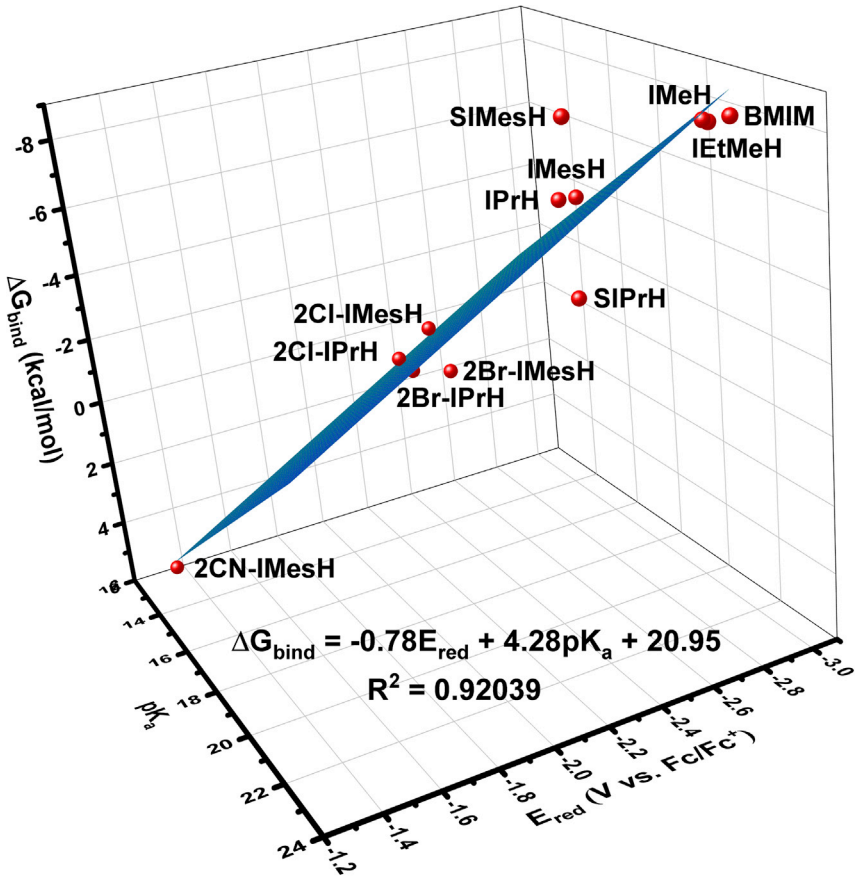

Figure 3. 3D correlation provides greater predictive power for estimating the free energy of CO_2 binding
Three-parameter linear relationship providing stronger correlation between E_{red}, pK_a, and ΔG_{bind} for the compounds under study

is used to estimate a ΔG_{bind} of −4.87 kcal/mol. These values compare favorably with the DFT-calculated ΔG_{bind} of −5.78 kcal/mol, yielding errors of 0.16 kcal/mol (3%) and 0.91 kcal/mol (15%), respectively, and bracketing the calculated value.

Alternatively, in the case of imidazol(in)ium cations for which both the experimental pK_a and E_{red} are known, Equation 3 (Figure 3),

$$\Delta G_{bind} = -0.78pK_a + 4.28E_{red} + 20.95 \quad \text{Equation 3}$$

is used to produce an estimated value for ΔG_{bind} with higher confidence than the individual correlations presented in Figure 2. For IMesH, this results in an estimated ΔG_{bind} of −5.44 kcal/mol. This again

Table 1. Comparison of DFT-calculated ΔG_{bind} values with those estimated using experimental reduction potentials and pK_a value

ImH	Exp. E_{red} (V vs. Fc/Fc^+)	Exp. pK_a	Est. ΔG_{bind} (kcal/mol)	DFT ΔG_{bind} (kcal/mol)	Error (%)
IMesH	−2.64	19.4	−5.4	−5.8	6
IPrH	−2.63	19.3	−5.3	−6.0	12
IMeH	−2.83	22.0	−8.3	−8.3	0.2
EtMeH	−2.87	22.1	−8.5	−8.2	4
BMIM	−2.84	22.0	−8.3	−8.4	1

Table 2. Comparison of estimated pK_a values from Equation 4 and experimental pK_a values

ImH	Exp. E_{red} (V vs. Fc/Fc^+)	Est. pK_a	Exp. pK_a	Error (%)
IMesH	−2.64	22.2	19.4	15
IPrH	−2.63	22.2	19.3	15
IMeH	−2.83	23.8	22.0	8
EtMeH	−2.87	24.1	22.1	9
BMIM	−2.84	23.9	22.0	8

compares favorably to the DFT-calculated value of ΔG_{bind}, this time yielding an error of only 0.34 kcal/mol (6%) and improving substantially upon the value obtained from the pK_a-only estimation. The results of using Equation 3 for all six compounds for which experimental values of E_{red} and pK_a are reported in Table 1.

Finally, as reduction potential is the most experimentally accessible value, it is desirable for various applications to predict the pK_a of an imidazol(in)ium cation from its measured E_{red}. To do this, the two-way correlation equation of Figure 2 *right* is used (Equation 4),

$$pK_a = -8.08E_{red} + 0.92 \qquad \text{Equation 4}$$

Table 2 below compares computed and experimental pK_as.

DISCUSSION

We now establish a three-way correlation between the reduction potential, pK_a, and free energy of CO_2 binding for a set of imidazol(in)ium cations and their corresponding NHCs and use it to demonstrate the facile calculation of CO_2 binding energies from experimentally accessible electrochemical measurements. Four halogenated NHCs known to be stable to oxygen, a necessary sorbent trait for carbon capture applications in which oxygen may be present, were predicted to bind CO_2 with negative values of ΔG_{bind}. Thermodynamic calculations for carbon capture (Petersen and Luca, 2021) suggest that materials that target energetically efficient reversible binding of CO_2 may be weak binders because strong binding results in a substantial energy penalty for the release phase. Although in this study we demonstrate our predictions on imidazol(in)ium-based NHCs, similar correlations will apply to other families of electrochemically responsive CO_2 capture molecular materials, thus enabling the mapping of energetics of a new chemical space for this application. Coupled with the known thermally triggered release of CO_2 from NHC-CO_2 adducts, our findings set the stage for energetic tuning of reactive separations in novel hybrid redox-thermal swing chemistries.

Limitations of the study

Strong ionic association may have an impact on observed reduction potentials, resulting in values that differ substantially from those predicted by the correlations presented herein. While the subset of organic salts investigated is limited, we expect the correlation to hold across a large library of chemically similar species. However, steric effects may cause significant deviations from the established trends, as has been observed in the case of 1,3-di-*t*-butylimidazolium chloride (I^tBuHCl).

STAR★METHODS

Detailed methods are provided in the online version of this paper and include the following:

- KEY RESOURCES TABLE
- RESOURCE AVAILABILITY
  - Lead contact
  - Materials availability
  - Data and code availability
- METHOD DETAILS
  - Electrochemical experiments
  - Computational data

SUPPLEMENTAL INFORMATION

Supplemental information can be found online at https://doi.org/10.1016/j.isci.2022.103997.

ACKNOWLEDGMENTS

We thank Prof. Xiao Su, Prof. Carl Koval, and Prof. Rich Noble for useful discussions. ORL thanks the University of Colorado for startup funds. AWA thanks Kuwait University for a graduate fellowship. HP thanks the University of Colorado Department of Chemistry for a summer 2021 research fellowship and the National Science Foundation Graduate Research Fellowship Program. This material is based upon work supported by the National Science Foundation Graduate Research Fellowship under Grant No. DGE 2040434.

AUTHOR CONTRIBUTIONS

The manuscript was written through contributions of all authors. ORL, AA, and HP wrote the manuscript. AA and CM contributed the computational section, HP, TS, and CH contributed the experimental section. All authors have given approval to the final version of the manuscript. These authors contributed equally.

DECLARATION OF INTERESTS

The authors declare no competing interests.

Received: November 5, 2021
Revised: December 28, 2021
Accepted: February 23, 2022
Published: April 15, 2022

REFERENCES

Alherz, A., Lim, C.-H., Kuo, Y.-C., Lehman, P., Cha, J., Hynes, J.T., and Musgrave, C.B. (2018). Renewable hydride donors for the catalytic reduction of CO_2: a thermodynamic and kinetic study. J. Phys. Chem. B *122*, 10179–10189.

Arduengo, A.J., Davidson, F., Dias, H.V.R., Goerlich, J.R., Khasnis, D., Marshall, W.J., and Prakasha, T.K. (1997). An air stable carbene and mixed carbene "dimers". J. Am. Chem. Soc. *119*, 12742–12749.

Barone, V., and Cossi, M. (1998). Quantum calculation of molecular energies and energy gradients in solution by a conductor solvent model. J. Phys. Chem. A *102*, 1995–2001.

Camaioni, D.M., and Schwerdtfeger, C.A. (2005). Comment on "accurate experimental values for the free energies of hydration of H^+, OH^-, and H_3O^+". J. Phys. Chem. A *109*, 10795–10797.

Chai, J.-D., and Head-Gordon, M. (2008). Long-range corrected hybrid density functionals with damped atom–atom dispersion corrections. Phys. Chem. Chem. Phys. *10*, 6615.

Chu, Y., Deng, H., and Cheng, J.-P. (2007). An acidity scale of 1,3-dialkylimidazolium salts in dimethyl sulfoxide solution. J. Org. Chem. *72*, 7790–7793.

Cossi, M., Rega, N., Scalmani, G., and Barone, V. (2003). Energies, structures, and electronic properties of molecules in solution with the C-PCM solvation model. J. Comput. Chem. *24*, 669–681.

Donadt, T.B., Lilio, A.M., Stinson, T.A., Lama, B., and Luca, O.R. (2018). DOSY NMR and normal pulse voltammetry for the expeditious determination of number of electrons exchanged in redox events. ChemistrySelect *3*, 7410–7415.

Dunn, M.H., Konstandaras, N., Cole, M.L., and Harper, J.B. (2017). Targeted and systematic approach to the study of pKa values of imidazolium salts in dimethyl sulfoxide. J. Org. Chem. *82*, 7324–7331.

Frisch, M.J., Trucks, G.W., Schlegel, H.B., Scuseria, G.E., Robb, M.A., Cheeseman, J.R., Scalmani, G., Barone, V., Petersson, G.A., Nakatsuji, H., et al. (2016). Gaussian 16 Rev. C.01, https://gaussian.com/citation/.

Furfari, S.K., Gyton, M.R., Twycross, D., and Cole, M.L. (2015). Air stable NHCs: a study of stereoelectronics and metallorganic catalytic activity. Chem. Commun. *51*, 74–76.

Gorodetsky, B., Ramnial, T., Branda, N.R., and Clyburne, J.A. (2004). Electrochemical reduction of an imidazolium cation: a convenient preparation of imidazol-2-ylidenes and their observation in an ionic liquid. Chem. Commun. *2004*, 1972–1973.

Hahn, F.E., and Jahnke, M.C. (2008). Heterocyclic carbenes: synthesis and coordination chemistry. Angew. Chem. Int. Ed. *47*, 3122–3172.

Ilic, S., Alherz, A., Musgrave, C.B., and Glusac, K.D. (2018). Thermodynamic and kinetic hydricities of metal-free hydrides. Chem. Soc. Rev. *47*, 2809–2836.

Institute, G.C. (2020). The Global Status of CCS: 2020 (Australia).

Isse, A.A., and Gennaro, A. (2010). Absolute potential of the standard hydrogen electrode and the problem of interconversion of potentials in different solvents. J. Phys. Chem. B *114*, 7894–7899.

Kelemen, Z., Hollóczki, O., Nagy, J., and Nyulászi, L. (2011). An organocatalytic ionic liquid. Org. Biomol. Chem. *9*, 5362–5364.

Kelly, C.P., Cramer, C.J., and Truhlar, D.G. (2006). Aqueous solvation free energies of ions and ion−water clusters based on an accurate value for the absolute aqueous solvation free energy of the proton. J. Phys. Chem. B *110*, 16066–16081.

Krishnan, R., Binkley, J.S., Seeger, R., and Pople, J.A. (1980). Self-consistent molecular orbital methods. XX. A basis set for correlated wave functions. J. Chem. Phys. *72*, 650–654.

Lackner, K.S. (2013). The thermodynamics of direct air capture of carbon dioxide. Energy *50*, 38–46.

Luca, O.R., and Fenwick, A.Q. (2015). Organic reactions for the electrochemical and photochemical production of chemical fuels from CO_2–The reduction chemistry of carboxylic acids and derivatives as bent CO_2 surrogates. J. Photochem. Photobiol. B Biol. *152*, 26–42.

Luca, O.R., McCrory, C.C., Dalleska, N.F., and Koval, C.A. (2015). The selective electrochemical conversion of preactivated CO_2 to methane. J. Electrochem. Soc. *162*, H473.

Marenich, A.V., Cramer, C.J., and Truhlar, D.G. (2009). Universal solvation model based on solute electron density and on a continuum model of the solvent defined by the bulk dielectric constant and atomic surface tensions. J. Phys. Chem. B *113*, 6378–6396.

Marenich, A.V., Ho, J., Coote, M.L., Cramer, C.J., and Truhlar, D.G. (2014). Computational electrochemistry: prediction of liquid-phase reduction potentials. Phys. Chem. Chem. Phys. *16*, 15068–15106.

McLean, A.D., and Chandler, G.S. (1980). Contracted gaussian basis sets for molecular calculations. I. second row atoms, Z=11–18. J. Chem. Phys. *72*, 5639–5648.

Mirzaei, S., Ivanov, M.V., and Timerghazin, Q.K. (2019). Improving performance of the SMD solvation model: bondi radii improve predicted aqueous solvation free energies of ions and pKa values of thiols. J. Phys. Chem. A *123*, 9498–9504.

Namazian, M., Lin, C.Y., and Coote, M.L. (2010). Benchmark calculations of absolute reduction potential of ferricinium/ferrocene couple in nonaqueous solutions. J. Chem. Theor. Comput. *6*, 2721–2725.

National Academies of Sciences, Engineering, and Medicine (2019). Negative Emissions Technologies and Reliable Sequestration: A Research Agenda (The National Academies Press).

Petersen, H.A., and Luca, O.R. (2021). Application-specific thermodynamic favorability zones for direct air capture of carbon dioxide. Phys. Chem. Chem. Phys. *23*, 12533–12536.

Riduan, S.N., Zhang, Y., and Ying, J.Y. (2009). Conversion of carbon dioxide into methanol with silanes over N-heterocyclic carbene catalysts. Angew. Chem. Int. Ed. *48*, 3322–3325.

Sowmiah, S., Srinivasadesikan, V., Tseng, M.-C., and Chu, Y.-H. (2009). On the chemical stabilities of ionic liquids. Molecules *14*, 3780–3813.

Thapa, B., and Schlegel, H.B. (2016). Density functional theory calculation of pKa's of thiols in aqueous solution using explicit water molecules and the polarizable continuum model. J. Phys. Chem. A *120*, 5726–5735.

Tossell, J.A. (2011). Calculation of the properties of molecules in the pyridine catalyst system for the photochemical conversion of CO_2 to methanol. Comput. Theor. Chem. *977*, 123–127.

Tsuzuki, S., Shinoda, W., Miran, M.S., Kinoshita, H., Yasuda, T., and Watanabe, M. (2013). Interactions in ion pairs of protic ionic liquids: comparison with aprotic ionic liquids. J. Chem. Phys. *139*, 174504.

Van Ausdall, B.R., Glass, J.L., Wiggins, K.M., Aarif, A.M., and Louie, J. (2009). A systematic investigation of factors influencing the decarboxylation of imidazolium carboxylates. J. Org. Chem. *74*, 7935–7942.

Voroshylova, I.V., Ferreira, E.S., Malček, M., Costa, R., Pereira, C.M., and Cordeiro, M.N.D. (2018). Influence of the anion on the properties of ionic liquid mixtures: a molecular dynamics study. Phys. Chem. Chem. Phys. *20*, 14899–14918.

Voutchkova, A.M., Feliz, M., Clot, E., Eisenstein, O., and Crabtree, R.H. (2007). Imidazolium carboxylates as versatile and selective N-heterocyclic carbene transfer agents: synthesis, mechanism, and applications. J. Am. Chem. Soc. *129*, 12834–12846.

Wang, H., Gu, S., Bai, Y., Chen, S., Zhu, N., Wu, C., and Wu, F. (2015). Anion-effects on electrochemical properties of ionic liquid electrolytes for rechargeable aluminum batteries. J. Mater. Chem. A *3*, 22677–22686.

Wang, Z., Wang, F., Xue, X.-S., and Ji, P. (2018). Acidity scale of N-heterocyclic carbene precursors: can we predict the stability of NHC–CO_2 adducts? Org. Lett. *20*, 6041–6045.

Wilcox, J. (2020). An electro-swing approach. Nat. Energy *5*, 121–122.

Yang, L., and Wang, H. (2014). Recent advances in carbon dioxide capture, fixation, and activation by using N-heterocyclic carbenes. ChemSusChem *7*, 962–998.

Yu, H.S., He, X., Li, S.L., and Truhlar, D.G. (2016). MN15: a kohn–sham global-hybrid exchange–correlation density functional with broad accuracy for multi-reference and single-reference systems and noncovalent interactions. Chem. Sci. *7*, 5032–5051.

Zhao, S.-F., Horne, M., Bond, A.M., and Zhang, J. (2016). Is the imidazolium cation a unique promoter for electrocatalytic reduction of carbon dioxide? The J. Phys. Chem. C *120*, 23989–24001.

STAR★METHODS

KEY RESOURCES TABLE

REAGENT or RESOURCE	SOURCE	IDENTIFIER
Chemicals, peptides, and recombinant proteins		
1,3-bis(2,4,6-trimethylphenyl)-imidazolium chloride (IMesHCl)	Strem Chemicals	Cat#07-0299; CAS-No. 141556-45-8
1,3-Bis(2,4,6-trimethylphenyl)-4,5-dihydroimidazolium chloride (SIMesHCl)	Strem Chemicals	Cat#07-4011; CAS-No. 173035-10-4
1,3-bis(2,6-diisopropylphenyl)-imidazolium chloride (IPrHCl)	Strem Chemicals	Cat#07-0590; CAS-No. 250285-32-6
1,3-bis(2,6-diisopropylphenyl)-4,5-dihydroimidazolium chloride (SIPrHCl)	TCI Chemicals	Cat# B3157; CAS-No. 258278-25-0
1,3-bis(2,6-diisopropylphenyl)-4,5-dihydroimidazolium tetrafluoroborate (SIPrH BF_4)	Sigma Aldrich	Cat# 693553-1G; CAS-No. 282109-83-5
1,3-dimethylimidazolium chloride (IMeHCl)	TCI Chemicals	Cat#D3341; CAS-No. 79917-88-7
1-ethyl-3-methylimidazolium hexafluorophosphate (IEtMeHCl)	Alfa Aesar	Cat# L19762; CAS-No. 155371-19-0
1,3-di-t-butylimidazolium chloride (I^tBuHCl)	Strem Chemicals	Cat#07-0368; CAS-No. 157197-54-1
1-butyl-3-methylimidazolium bis(trifluoromethylsulfonyl)imide (BMIM TFSI)	Sigma Aldrich	Cat#77896-1G-F; CAS-No. 174899-83-3
Tetrabutylammonium hexafluorophosphate	Sigma Aldrich	Cat#86874-100G; CAS-No. 3109-63-5
Acetonitrile	Pharmco	Cat#300000DIS; CAS-No. 75-05-8
Methanol	Macron Fine Chemicals	Cat#3016-16; CAS-No. 67-56-1
Software and algorithms		
MN15 Functional	Yu et al., 2016	N/A
6-311+G(d,p) Basis Set	Krishnan et al., 1980	N/A
SMD Solvent Model	Marenich et al., 2009	N/A
McLean-Chandler (12s,9p) → (621111,52111) basis sets	McLean and Chandler, 1980	N/A
ωB97X-D Functional	Chai and Head-Gordon, 2008	N/A
CPCM Solvent Model	Barone and Cossi, 1998	N/A
Gaussian 16	Frisch et al., 2016	N/A
Optimized molecular coordinates	Data S1	Used in Figure 2
OriginPro 2019b	OriginLab	N/A

RESOURCE AVAILABILITY

Lead contact

Further information and requests for resources and reagents should be directed to and will be fulfilled by the lead contact, Oana Luca (oana.luca@colorado.edu).

Materials availability

This study did not generate new unique reagents.

Data and code availability

All data reported in this paper will be shared by the lead contact upon request. This paper does not report original code. Any additional information required to reanalyze the data reported in this paper is available from the lead contact upon request. Optimized molecular coordinates used in the Figure 2 analysis are available for download as Data S1.

METHOD DETAILS

Electrochemical experiments

General methods

Reagents for use in electrochemical experiments were purchased from commercial sources and used as received except where otherwise noted. 1,3-bis(2,4,6-trimethylphenyl) imidazolium chloride (IMesHCl), 1,3-Bis(2,4,6-trimethylphenyl)-4,5-dihydroimidazolium chloride (SIMesHCl), 1,3-bis(2,6-diisopropylphenyl) imidazolium chloride (IPrHCl), 1,3-bis(2,6-diisopropylphenyl)-4,5-dihydroimidazolium chloride (SIPrHCl), 1,3-bis(2,6-diisopropylphenyl)-4,5-dihydroimidazolium tetrafluoroborate (SIPrH BF_4), 1,3-dimethylimidazolium chloride (IMeHCl), 1-ethyl-3-methylimidazolium hexafluorophosphate (IEtMeHCl), 1,3-di-t-butylimidazolium chloride (I^tBuHCl), and 1-butyl-3-methylimidazolium bis(trifluoromethylsulfonyl)imide (BMIM TFSI) were purchased commercially. Acetonitrile (MeCN) used in electrochemical experiments was freshly distilled and sparged with argon before use. Tetrabutylammonium hexafluorophosphate (NBu_4 PF_6) was recrystallized from methanol and dried overnight under high vacuum before use as supporting electrolyte.

Normal Pulse Voltammetry (NPV) experiments were performed using a silver wire single junction pseudo-reference electrode, a 3 mm diameter glassy carbon working electrode (MF-2012, BASI), and a platinum wire counter electrode. Standard NPV experimental conditions were 50 ms pulse width, 200 ms step time, and −10 mV pulse height. A vial filled with MeCN was used as a pre-bubbler to prevent solvent evaporation over the course of the experiment. Each imidazolium salt was dissolved in a 0.1 M NBu_4 PF_6 solution in MeCN and was degassed with argon prior to analysis. All glassware and needles used in the experiment and in solution transfer were oven-dried prior to use, and solvents and supporting electrolyte were dried as described above. The ferrocene/ferrocenium couple was used as an external standard reference for the applied potential.

Experimental reduction potentials

Each imidazolium salt was dissolved as a 1 mM solution in acetonitrile with 0.1 M NBu_4 PF_6 and subjected to the standard NPV conditions described above. The chloride salt was used for each imidazolium of interest, with the exception of BMIM TFSI. Experimental imidazolium reduction potentials were obtained by finding the potential at which the inflection point occurs in the NPV of the compound in question. This method was chosen over standard use of cyclic voltammetry $E_{1/2}$ values due to the irreversible nature of the reduction and the improved ability of NPV to provide precise current responses with minimal interference from charging currents. This value was then averaged across three trials (with the exception of SIPr, 6 trials).

Electron quantification

NPV was used to determine the number of electrons associated with the reduction of SIPr using the method of Donadt et al. The number of electrons associated with a given electrochemical feature can be calculated using the Cottrell Equation, $i_l = \frac{nFAC_o\sqrt{D}}{\sqrt{\pi t}}$, in which i_l is limiting current (the current at the plateau of a feature), n is the number of electrons associated with the feature, F is Faraday'|'s constant, A is the electrode surface area, C_o is the bulk concentration of the analyte, D is the diffusion coefficient of the analyte, and t is the pulse width. The diffusion coefficient of SIPrH was first obtained by conducting Diffusion-Ordered SpectroscopY (DOSY) NMR on a sample of SIPrH BF_4 in deuterated MeCN. The diffusion coefficient was found to be $1.11*10^{-5}$ cm^2/s. NPV (Figure S2) was then collected using a sample of 3.53 mg of the imidazolium salt IPrH BF_4 dissolved in a known amount of MeCN. The total sample mass was obtained before and just after the experiment to account for solvent loss during degassing and was used to calculate a final bulk concentration of 1.68 mM. Using the geometric electrode surface area of the 3 mm glassy carbon working electrode and the respective time parameter for each scan, the value of n can then be obtained with the Cottrell Equation.

Computational data

General methods

Quantum chemical density functional theory calculations have been conducted to compute the optimized geometries and energies of the carbene precursor, its protonated and reduced intermediates, and their adducts with CO_2. Frequency calculations were performed to ensure that the optimized geometries have no imaginary frequencies and obtain thermal and entropic corrections to the electronic energy to calculate Gibbs free energies. The DFT calculations utilize the Minnesota 15 (MN15) functional, Pople basis sets with polarization and diffuse functions 6-311+G(d,p), and acetonitrile solvent as described by the SMD

solvent model (Krishnan et al., 1980; Marenich et al., 2009; McLean and Chandler, 1980; Yu et al., 2016) implemented within the Gaussian 16 software (Frisch et al., 2016). The energies obtained are used to calculate 3 main observable properties: pK_a values, reduction potentials (of the protonated carbene intermediate), and the free energies of binding CO_2 to the resultant carbenes.

Similar computations were performed using the wB97xD/6-311+G(d,p)/CPCM method for comparison (Barone and Cossi, 1998; Chai and Head-Gordon, 2008; Cossi et al., 2003). The default cavity settings were additionally modified, as recommended by Mirzaei et al. (Mirzaei et al., 2019), such that the atomic radii for cavity estimates are modelled according to the Bondi radii rather than the fitted SMD-Coulomb parameters, and the calculations were carried out again. The three overall computational methods compared herein are therefore MN15/6-311+G(d,p)/SMD, MN15/6-311+G(d,p)/SMD-Bondi, and wB97xD/6-311+G(d,p)/CPCM.

All three DFT methods investigated are rather accurate in predicting pK_a values compared to experimental values obtained from Ref. 18, as shown in Table S2. While the pK_a and E_{red} values of I^{t}BuH were accurately predicted, this imidazolium was omitted from the correlation plots because it deviates significantly from the trends obeyed by the other species where its computed ΔG_{bind} value deviates by more than 6 and 7 kcal/mol from the expected values provided by the E_{red} and pK_a correlations, respectively. This significantly different behavior most likely stems from the bulky ^{t}Bu groups of I^{t}BuH that hinder CO_2 binding more than planar Ph-based or smaller alkyl groups, resulting in a much less favorable ΔG_{bind} value at comparable E_{red} and pK_a values that are not shifted so dramatically because electron and proton transfers are not hindered as much as CO_2 binding.

While the SMD-Bondi cavity treatment has not been benchmarked rigorously in literature, we find that it succeeds in providing accurate pK_a and E_{red} values (Tables S2 and S3), probably due to the nature of our fitting techniques discussed below. However, it seems to significantly over-stabilize the binding energies of CO_2 to carbenes. The SMD-Bondi cavity treatment significantly exaggerates the likelihood of binding (Table S4). Since this cavity method is the least tested across different systems and thus least trustworthy, we concluded that the default SMD treatment with the MN15 functional provides more realistic binding free energy values and opted to use this method for our correlations. It is also more in agreement with the well-established wB97xD/CPCM method, within expected DFT errors (MAE = 3.2 kcal/mol).

Acidity (pK_a)

pK_a values are obtained by creating a linear fit between experimentally determined pK_a values and the computed free energy difference $G(XH^+) - G(X)$. While it is common to estimate pK_a values using an isodesmic approach or use a pre-determined free energy of solvated protons $G(H^+)$ (Alherz et al., 2018; Thapa and Schlegel, 2016), we argue that a linear fitting approach avoids any systematic errors in pK_a predictions. Figure S3 shows the linear correlation described. The linear correlation is used to predict pK_a values for other carbenes by computing the energies of the XH^+ and X intermediates. This computation is performed for the energies obtained from each of the three DFT levels of theory for each imidazolium (Table S4). This can also be used to extrapolate the expected free energy of an acetonitrile-solvated proton, $G(H^+) = -263.4 \frac{kcal}{mol}$, in close agreement with the experimentally determined value of −265.9 kcal/mol (Camaioni and Schwerdtfeger, 2005; Isse and Gennaro, 2010; Kelly et al., 2006; Marenich et al., 2014).

Reduction potentials (E_{red})

Reduction potentials are first calculated according to the equation $E^0 = G_{X^+} - G_{X^\bullet} - E^0_{ref}$, where E^0_{ref} is the absolute redox potential of the ferrocene/ferrocenium reference couple (4.988 V in acetonitrile) (Namazian et al., 2010; Tossell, 2011). To avoid systematic underestimation of E_{red} (−0.3 V vs. experimental values), we then utilize a linear fitting approach between experimentally determined E_{red} values and the free energy differences $G(X^\bullet) - G(X^+)$. This computation is performed for the energies obtained from each of the three DFT levels of theory for each imidazolium (Table S4).

CO_2 binding free energy

The free energy of CO_2 binding is computed according to the equation $\Delta G_{binding} = G(XCO_2) - G(X:) - G(CO_2)$, where $G(XCO_2)$ is the free energy of the NHC-CO_2 adduct, $G(X:)$ is the free energy of the free

NHC, and $G(CO_2)$ is the free energy of free CO_2. This computation is performed for the energies obtained from each of the three DFT levels of theory for each imidazolium (Table S4).

Coordinates

Data S1: Optimized molecular coordinates. All optimized molecular coordinates (MN15/6-311+G(d,p)/SMD level of theory) for the carbenes and intermediates of interest used in Figure 2 are provided in.xyz format as a supplemental data.

Correlation

Best-fit analyses of each of the correlated parameters (E_{red} vs. pK_a, E_{red} vs. ΔG_{bind}, pK_a vs. ΔG_{bind}, and E_{red} vs. pK_a vs. ΔG_{bind}) were carried out in OriginPro 2019b.